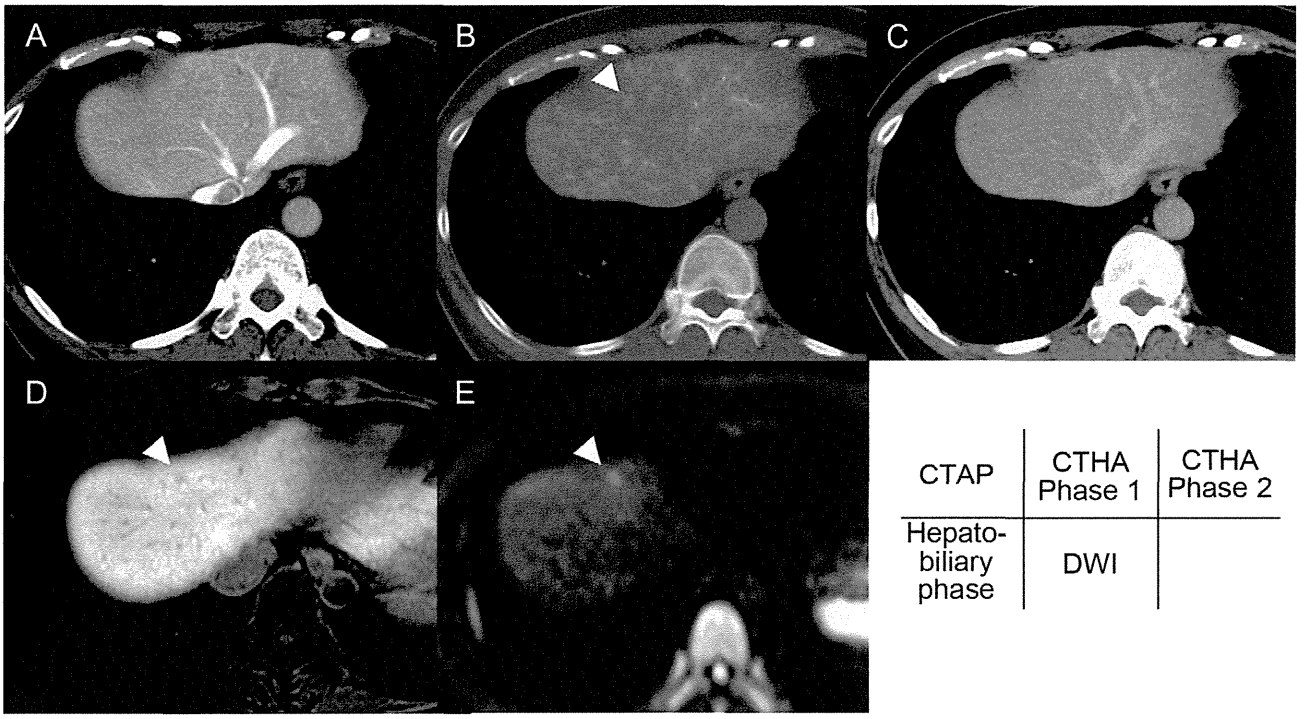

Fig. 2. The white arrow shows another HCC from the same patient as in Fig. 1. It was also proven in the resected specimen. The HCC shows low intensity in the hepatobiliary phase (D) and high signal on DWI (E). In the retrospective review, it was slightly enhanced on first-phase CTHA (B). The HCC was detected by none of the readers in the CTAP/CTHA set (A–C), but by all three readers in the gadoxetic acid-enhanced MRI set and scored as 4.

As in the previous report, our data also indicate clearly that both CTAP/CTHA and comprehensive gadoxetic acid-enhanced MRI have high sensitivity and diagnostic accuracy. Importantly, the diagnostic accuracy of gadoxetic acid-enhanced MRI was significantly higher than that of CTAP/CTHA. The sensitivity of gadoxetic acid-enhanced MRI was also higher than that of CTAP/CTHA. The positive predictive value, negative predictive value and specificity were similar between the two modalities. These results support the previous report and demonstrate the superiority of gadoxetic acid-enhanced MRI to CTAP/CTHA not only for patients with very good liver function who can undergo resection, but also for those with relatively poor liver function.

In some cases, DWI increased the confidence in the result. This concurs with the finding that multi-sequence MRI including DWI improved the HCC diagnostic performance [21,22].

This study had several limitations. First, the patient population was collected retrospectively, and there may have been some selection bias. We analyzed patients with pathologically proven HCC nodules, and some patients who were diagnosed only with a radiological examination but without pathological proof were excluded from our study population. In particular, patients with no indication for both resection and local ablation therapy were excluded; there may have been few intrahepatic metastases of HCC in this study. This may have led to an overestimation of the sensitivity and positive predictive

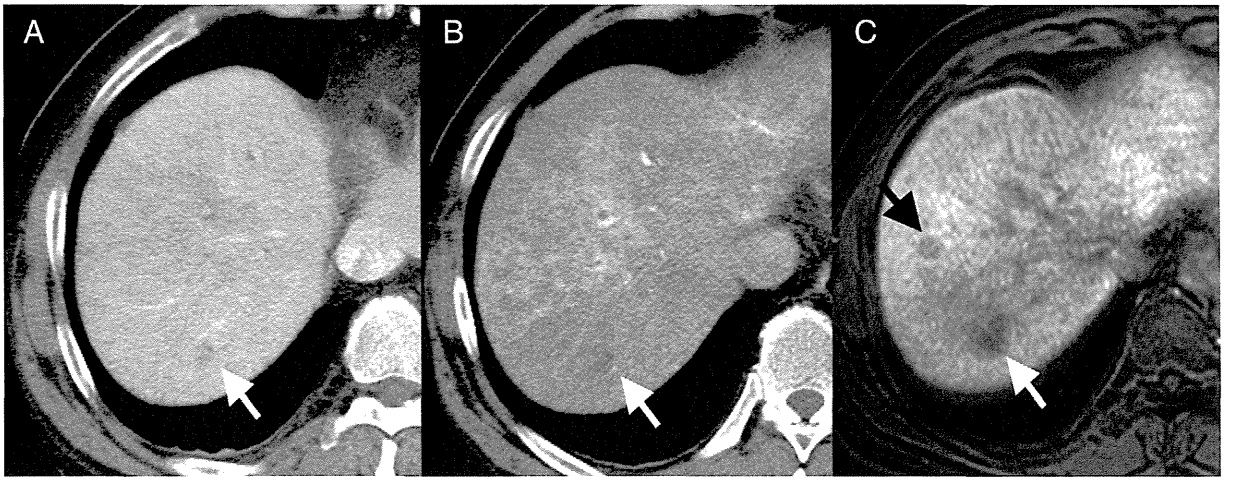

Fig. 3. Images from a 61-year-old male with hepatitis C cirrhosis and two biopsy-proven, well-differentiated HCCs. The white and black arrows show the two well-differentiated HCCs. The white arrow shows a hypoattenuating nodule on CTAP (A) and on second-phase CTHA (B). This lesion became hypointense on the gadoxetic acid-enhanced image obtained during the hepatobiliary phase. All three readers detected this lesion as HCC on both the CTAP/CTHA and gadoxetic acid-enhanced MRI image sets. The other HCC was difficult to detect on CTAP/CTHA, even retrospectively. This HCC was detected only on the gadoxetic acid-enhanced image obtained during the hepatobiliary phase (c), and all three readers assigned this lesion a score of 3.

value. Second, the negative lesions were not proven pathologically. We did not perform biopsies in all unchanged nodules because there was a probability of causing a sampling error at biopsy of small hepatic lesions, and pathological diagnosis may be difficult because of intratumoral heterogeneity. Therefore, a positive biopsy is helpful, but a negative biopsy cannot be proof of a negative lesion. If patients who could not undergo surgical resection because of poor hepatic function were included in the study population, this limitation could be avoided, with the exception of the use of explanted livers. Third, all three readers were aware that all of the patients had HCC, and this might have resulted in high sensitivities and positive predictive values. Fourth, no patients had advanced or end-stage cirrhosis and/or HCC in our study, which might also have affected the diagnostic performance.

Our data suggest that a comprehensive evaluation using gadoxetic acid-enhanced MRI including a gradient dual-echo sequence and DWI is superior to CTAP/CTHA for the pre-therapeutic detection of HCC, regardless of nodule size. Furthermore, gadoxetic acid-enhanced MRI does not require hospitalization and is less invasive than CTAP/CTHA. A comprehensive assessment using gadoxetic acid-enhanced MRI is recommended in the pre-therapeutic evaluation to HCC patients.

Acknowledgments

The authors thank Hideyuki Kato and Yoshitada Masuda for their contributions.

References

[1] El-Serag HB, Rudolph KL. Hepatocellular carcinoma: epidemiology and molecular carcinogenesis. Gastroenterology 2007;132(7):2557-76.
[2] Bruix J, Sherman M. Practice Guidelines Committee AAftSoLD. Management of hepatocellular carcinoma. Hepatology (Baltimore, MD) 2005;42(5):1208-36.
[3] Yuen MF, Cheng CC, Lauder IJ, Lam SK, Ooi CG, Lai CL. Early detection of hepatocellular carcinoma increases the chance of treatment: Hong Kong experience. Hepatology (Baltimore, MD) 2000;31(2):330-5.
[4] Matsui O, Takashima T, Kadoya M, Ida M, Suzuki M, Kitagawa K, et al. Dynamic computed tomography during arterial portography: the most sensitive examination for small hepatocellular carcinomas. J Comput Assist Tomogr 1985;9(1):19-24.
[5] Yukisawa S, Okugawa H, Masuya Y, Okabe S, Fukuda H, Yoshikawa M, et al. Multidetector helical CT plus superparamagnetic iron oxide-enhanced MR imaging for focal hepatic lesions in cirrhotic liver: a comparison with multiphase CT during hepatic arteriography. Eur J Radiol 2007;61(2):279-89.
[6] Jang HJ, Lim JH, Lee SJ, Park CK, Park HS, Do YS. Hepatocellular carcinoma: are combined CT during arterial portography and CT hepatic arteriography in addition to triple-phase helical CT all necessary for preoperative evaluation? Radiology 2000;215(2):373-80.
[7] Imai Y, Murakami T, Hori M, Fukuda K, Kim T, Marukawa T, et al. Hypervascular hepatocellular carcinoma: combined dynamic MDCT and SPIO-enhanced MRI versus combined CTHA and CTAP. Hepatol Res 2008;38(2):147-58.
[8] Inoue E, Fujita M, Hosomi N, Sawai Y, Hashimoto T, Kuroda C, et al. Double-phase CT arteriography of the whole liver in the evaluation of hepatic tumors. J Comput Assist Tomogr 1998;22(1):64-8.
[9] Murakami T, Takamura M, Kim T, Hori M, Federle MP, Onishi H, et al. Double-phase CT during hepatic arteriography for diagnosis of hepatocellular carcinoma. Eur J Radiol 2005;54(2):246-52.
[10] Hamm B, Staks T, Muhler A, Bollow M, Taupitz M, Frenzel T, et al. Phase I clinical evaluation of Gd-EOB-DTPA as a hepatobiliary MR contrast agent: safety, pharmacokinetics, and MR imaging. Radiology 1995;195(3):785-92.
[11] Ahn SS, Kim MJ, Lim JS, Hong HS, Chung YE, Choi JY. Added value of gadoxetic acid-enhanced hepatobiliary phase MR imaging in the diagnosis of hepatocellular carcinoma. Radiology 2010;255(2):459-66.
[12] Chou CT, Chen YL, Wu HK, Chen RC. Characterization of hyperintense nodules on precontrast T1-weighted MRI: utility of gadoxetic acid-enhanced hepatocyte-phase imaging. J Magn Reson Imaging 2011;33(3):625-32.
[13] Bluemke DA, Sahani D, Amendola M, Balzer T, Breuer J, Brown JJ, et al. Efficacy and safety of MR imaging with liver-specific contrast agent: U.S. multicenter phase III study. Radiology 2005;237(1):89-98.
[14] Halavaara J, Breuer J, Ayuso C, Balzer T, Bellin MF, Blomqvist L, et al. Liver tumor characterization: comparison between liver-specific gadoxetic acid disodium-enhanced MRI and biphasic CT—a multicenter trial. J Comput Assist Tomogr 2006;30(3):345-54.
[15] Kim YK, Kim CS, Han YM, Kwak HS, Jin GY, Hwang SB, et al. Detection of hepatocellular carcinoma: gadoxetic acid-enhanced 3-dimensional magnetic resonance imaging versus multi-detector row computed tomography. J Comput Assist Tomogr 2009;33(6):844-50.
[16] Ichikawa T, Saito K, Yoshioka N, Tanimoto A, Gokan T, Takehara Y, et al. Detection and characterization of focal liver lesions: a Japanese phase III, multicenter comparison between gadoxetic acid disodium-enhanced magnetic resonance imaging and contrast-enhanced computed tomography predominantly in patients with hepatocellular carcinoma and chronic liver disease. Invest Radiol 2010;45(3):133-41.
[17] Di Martino M, Marin D, Guerrisi A, Baski M, Galati F, Rossi M, et al. Intraindividual comparison of gadoxetate disodium-enhanced MR imaging and 64-section multidetector CT in the detection of hepatocellular carcinoma in patients with cirrhosis. Radiology 2010;256(3):806-16.
[18] Onishi H, Kim T, Imai Y, Hori M, Nagano H, Nakaya Y, et al. Hypervascular hepatocellular carcinomas: detection with gadoxetate disodium-enhanced MR imaging and multiphasic multidetector CT. Eur Radiol 2012;22(4):845-54.
[19] Akai H, Kiryu S, Matsuda I, Satou J, Takao H, Tajima T, et al. Detection of hepatocellular carcinoma by Gd-EOB-DTPA-enhanced liver MRI: comparison with triple phase 64 detector row helical CT. Eur J Radiol 2011;80(2):310-5.
[20] Martin J, Sentis M, Zidan A, Donoso L, Puig J, Falco J, et al. Fatty metamorphosis of hepatocellular carcinoma: detection with chemical shift gradient-echo MR imaging. Radiology 1995;195(1):125-30.
[21] Xu PJ, Yan FH, Wang JH, Lin J, Ji Y. Added value of breathhold diffusion-weighted MRI in detection of small hepatocellular carcinoma lesions compared with dynamic contrast-enhanced MRI alone using receiver operating characteristic curve analysis. JMRI 2009;29(2):341-9.
[22] Vandecaveye V, De Keyzer F, Verslype C, Op de Beeck K, Komuta M, Topal B, et al. Diffusion-weighted MRI provides additional value to conventional dynamic contrast-enhanced MRI for detection of hepatocellular carcinoma. Eur Radiol 2009;19(10):2456-66.
[23] Sano K, Ichikawa T, Motosugi U, Sou H, Muhi AM, et al. Imaging study of early hepatocellular carcinoma: usefulness of gadoxetic acid-enhanced MR imaging. Radiology 2011;261(3):834-44.
[24] Dorfman DD, Berbaum KS, Metz CE. Receiver operating characteristic rating analysis. Generalization to the population of readers and patients with the jackknife method. Invest Radiol 1992;27(9):723-31.
[25] Hillis SL, Obuchowski NA, Schartz KM, Berbaum KS. A comparison of the Dorfman-Berbaum-Metz and Obuchowski-Rockette methods for receiver operating characteristic (ROC) data. Stat Med 2005;24(10):1579-607.
[26] Golfieri R, Renzulli M, Lucidi V, Corcioni B, Trevisani F, Bolondi L. Contribution of the hepatobiliary phase of Gd-EOB-DTPA-enhanced MRI to dynamic MRI in the detection of hypovascular small (≤2 cm) HCC in cirrhosis. Eur Radiol 2011;21(6):1233-42.

OPEN ACCESS Freely available online

PLOS ONE

Disulfiram Eradicates Tumor-Initiating Hepatocellular Carcinoma Cells in ROS-p38 MAPK Pathway-Dependent and -Independent Manners

Tetsuhiro Chiba[1,2*☯], Eiichiro Suzuki[1,2☯], Kaori Yuki[1,2], Yoh Zen[3], Motohiko Oshima[2], Satoru Miyagi[2], Atsunori Saraya[2], Shuhei Koide[2], Tenyu Motoyama[1], Sadahisa Ogasawara[1], Yoshihiko Ooka[1], Akinobu Tawada[1], Tetsuya Nakatsura[4], Takehiro Hayashi[5], Taro Yamashita[5], Syuichi Kaneko[5], Masaru Miyazaki[6], Atsushi Iwama[2], Osamu Yokosuka[1]

1 Department of Gastroenterology and Nephrology, Graduate School of Medicine, Chiba University, Chiba, Japan, **2** Department of Cellular and Molecular Medicine, Graduate School of Medicine, Chiba University, Chiba, Japan, **3** Institute of Liver Studies, King's College Hospital, Denmark Hill, London, United Kingdom, **4** Division of Cancer Immunotherapy, Research Center for Innovative Oncology, National Cancer Center Hospital East, Kashiwa, Japan, **5** Department of Gastroenterology, Graduate School of Medicine, Kanazawa University, Kanazawa, Japan, **6** Department of General Surgery, Graduate School of Medicine, Chiba University, Chiba, Japan

Abstract

Tumor-initiating cells (TICs) play a central role in tumor development, metastasis, and recurrence. In the present study, we investigated the effect of disulfiram (DSF), an inhibitor of aldehyde dehydrogenase, toward tumor-initiating hepatocellular carcinoma (HCC) cells. DSF treatment suppressed the anchorage-independent sphere formation of both HCC cells. Flow cytometric analyses showed that DSF but not 5-fluorouracil (5-FU) drastically reduces the number of tumor-initiating HCC cells. The sphere formation assays of epithelial cell adhesion molecule (EpCAM)$^+$ HCC cells co-treated with p38-specific inhibitor revealed that DSF suppresses self-renewal capability mainly through the activation of reactive oxygen species (ROS)-p38 MAPK pathway. Microarray experiments also revealed the enrichment of the gene set involved in p38 MAPK signaling in EpCAM$^+$ cells treated with DSF but not 5-FU. In addition, DSF appeared to downregulate *Glypican 3* (*GPC3*) in a manner independent of ROS-p38 MAPK pathway. GPC3 was co-expressed with EpCAM in HCC cell lines and primary HCC cells and *GPC3*-knockdown reduced the number of EpCAM$^+$ cells by compromising their self-renewal capability and inducing the apoptosis. These results indicate that DSF impaired the tumorigenicity of tumor-initiating HCC cells through activation of ROS-p38 pathway and in part through the downregulation of *GPC3*. DSF might be a promising therapeutic agent for the eradication of tumor-initiating HCC cells.

Citation: Chiba T, Suzuki E, Yuki K, Zen Y, Oshima M, et al. (2014) Disulfiram Eradicates Tumor-Initiating Hepatocellular Carcinoma Cells in ROS-p38 MAPK Pathway-Dependent and -Independent Manners. PLoS ONE 9(1): e84807. doi:10.1371/journal.pone.0084807

Editor: Terence Lee, University of Hong Kong, Hong Kong

Received September 26, 2013; **Accepted** November 18, 2013; **Published** January 13, 2014

Funding: This work was supported in part by grants for the Global COE program (Global Center for Education and Research in Immune System Regulation and Treatment) from the Ministry of Education, Culture, Sports, Science and Technology, Japan (http://www.jsps.go.jp/j-globalcoe/); grants from Core Research for Evolutional Science and Technology (CREST) of Japan Science and Technology Corporation (JST)(http://www.jst.go.jp/kisoken/crest/); and the Foundation for the Promotion of Cancer Research (http://www.fpcr.or.jp/). The funders had no role in study design, data collection and analysis, decision to publish, or preparation of the manuscript.

Competing Interests: Prof. Osamu Yokosuka received grant support from Mitsubishi Tanabe Pharma. Dr. Taro Yamashita, an academic editor of PLOS ONE, is listed as a co-author of the manuscript. This does not alter the authors' adherence to all the PLOS ONE policies on sharing data and materials.

* E-mail: techiba@faculty.chiba-u.jp

☯ These authors contributed equally to this work.

Introduction

Accumulating evidence has revealed that a minor population of tumor cells, called cancer stem cells or tumor-initiating cells (TICs), organizes a cellular hierarchy in a similar fashion to normal stem cells and shows pronounced tumorigenic activity in xenograft transplantations [1]. Recent progress in stem cell biology and technologies has contributed to the identification and characterization of TICs in various cancers including hepatocellular carcinoma (HCC) [2]. In HCC, side population cells and cells expressing several surface molecules such as epithelial cell adhesion molecule (EpCAM), CD133, CD90, and CD13 have been reported to function as TICs [3]. Besides the identification of tumor-initiating HCC cells, cancer-related molecules and signaling pathways, such as the polycomb group proteins, NANOG, AKT/PKB signal, and Wnt/β-catenin, have been shown to play an important role in maintaining or augmenting of tumor-initiating capability of TICs [4]. Although inhibitors of these molecules and signaling pathways may be potent TIC-targeting drugs, no effective therapy targeting TICs has been developed.

Disulfiram (DSF) is an irreversible inhibitor of aldehyde dehydrogenase and has been clinically used in the treatment of alcohol dependence for roughly 70 years [5]. DSF is a potent therapeutic agent in a wide range of human cancers. In addition, recent reports showed that DSF reduced the number of tumor-initiating cells and attenuated their sphere-forming abilities in breast cancer and glioblastoma [6,7]. Although these findings

indicate that DSF could eradicate TICs, the molecular machinery of its effect against TICs still remains largely unknown.

In the present study, we examined the effects of DSF on tumor-initiating HCC cells *in vitro* and *in vivo*. We found that DSF impaired their tumor-initiating ability and induced apoptosis by activating the reactive oxygen species (ROS)-p38 pathway. Furthermore, the downregulation of *Glypican3 (GPC3)* expression, which is caused independently of the ROS-p38 pathway, appeared to also be responsible for the anti-TIC effect of DSF.

Results

DSF inhibited tumorigenicity of HCC cells *in vitro* and in a xenograft transplantation model

As shown in a variety of cancer cells [8–10], DSF treatment inhibited cell growth in both a time-dependent and dose-dependent manner in HCC cells (Figure S1A). Immunostaining of active caspase-3 (CASP3) showed that the DSF treatment induced apoptosis dose-dependently (Figure S1B). The percentage of apoptotic cells was roughly ten-fold higher among HCC cells treated with DSF (1 μM) than among control cells (Figure S1C). To examine whether DSF affected the tumorigenic ability of HCC cells, we conducted a non-adherent sphere assay, a standard assay for evaluating tumorigenic capacity. Sphere-forming ability was significantly impaired in DSF-treated HCC cell lines in a dose-dependent manner (Figure 1A and 1B). Subsequently, we determined the effects of DSF using a xenograft nonobese diabetic/severe combined immunodeficient (NOD/SCID) mouse model. After the implantation of 2×10^6 Huh1 and Huh7 cells into NOD/SCID mice, DSF was administered intraperitoneally every other day. Tumor initiation and growth were apparently suppressed by the DSF treatment in a dose-dependent manner (Figure 1C and 1D). Together, these results indicate that DSF reduced the tumorigenicity of HCC cells.

Loss-of-function assays of ALDH1 and ALDH2

DSF and its metabolites were shown to suppress ethanol metabolism mainly through the inhibition of cytosolic aldehyde dehydrogenase 1 (ALDH1) and mitochondrial ALDH2 [11]. It has been reported that *ALDH*-knockdown reduced proliferation and motility of lung cancer cells [12]. Because we previously showed that there was no association between the expression of ALDH1 and EpCAM or CD13 and that *ALDH1*-knockdown affected neither cell growth nor tumorigenicity in HCC cells [13], we conducted loss-of-function assays on ALDH2. We achieved the stable knockdown of *ALDH2* in Huh1 and Huh7 cells with lentivirus-mediated short hairpin RNA (shRNA) against *ALDH2* using enhanced red fluorescent protein (ERP) as a marker for infection (Figure S2A). No significant differences in cell growth and sphere formation were observed between *ALDH2*-knockdown cells and control cells expressing shRNA against *luciferase* (sh-*Luc*) (Figure S2B and S2C). Additionally, double-knockdown of *ALDH1* and *ALDH2* in the culture produced similar results to the single-knockdown of ALDH2 (Figure S2D-F). Taken together, the effects of DSF on HCC cells appeared to be independent of its inhibitory function toward ALDH1 and ALDH2.

Decrease in the number of tumor-initiating HCC cells after DSF exposure

We then examined the expression of various markers of tumor-initiating HCC cells such as CD13, epithelial cell adhesion molecule (EpCAM), and CD133 using flow cytometry. The DSF treatment appeared to decrease the number of HCC cells expressing these markers (Figure 2A). Among them, the EpCAM^{high} fraction markedly decreased from 44.4% to 9.8% in Huh1 cells and from 36.7% to 12.5% in Huh7 cells. Concordant with this, real-time RT-PCR analysis showed decreased expression of E-cadherin (CDH1) and alfa-fetoprotein (AFP), hepatic stem/progenitor cell markers, in DSF-treated cells (Figure 2B). In clear contrast, the 5-FU treatment resulted in the enrichment of TIC fractions (Figure S3). These results indicate that the biological effect of DSF differs from that of 5-FU, and is promising for the eradication of tumor-initiating HCC cells.

DSF activated p38 MAPK in response to increased intracellular ROS levels in tumor-initiating HCC cells

Consistent with previous reports [6,7], the present flow cytometric analyses showed that intracellular ROS levels were higher in DSF-treated HCC cells than in control cells (Figure 3A). However, co-treatment with NAC canceled this increase in ROS levels (Figure 3A). Western blotting showed increased levels of phosphorylated p38 after DSF exposure, which indicates p38 MAPK activation in HCC cells (Figure 3B). It has been well established that TICs maintain ROS at levels as low as normal stem cells [14,15]. ROS levels were higher in EpCAM$^-$ HCC cells than in EpCAM$^+$ cells (Figure 3C). Notably, the co-treatment of sorted EpCAM$^+$ cells with the antioxidant, NAC, canceled the phosphorylation of p38 induced by DSF (Figure 3D). Although EpCAM$^-$ HCC cells generated only a small number of spheres, DSF treatment further reduced the number of spheres (Figure S4A and S4B). Approximately 90% of EpCAM$^+$ cells treated with DSF was positive for phosphorylated p38 (Figure 3D), but the rate for EpCAM$^-$ cells positive for phosphorylated p38 was nearly 25% (Figure S4C). The cell growth of EpCAM$^+$ HCC cells was greatly restored by the additional NAC treatment (Figure 3E). Together, DSF caused activation of the ROS-p38 MAPK pathway in tumor-initiating HCC cells.

p38 MAPK activation impaired self-renewal capability of tumor-initiating HCC cells

To examine the impact of p38 MAPK activation on tumor-initiating HCC cells, we conducted sphere formation assays on EpCAM$^+$ HCC cells treated with DSF and/or SB203580, a specific inhibitor of p38 (Figure 4A). The co-treatment of cells with SB203580 largely abrogated the cell growth inhibition and apoptosis observed following the DSF treatment (Figure S5). Consistent with this, additional SB203580 treatment significantly restored the sphere-forming ability of EpCAM$^+$ HCC cells (Figure 4B). Additionally, subsequent analyses for secondary sphere formation after replating showed results similar to those for the primary spheres (Figure 4C). These results indicate that activated p38 MAPK restricts the self-renewal of tumor-initiating HCC cells. We then conducted immunocytochemical analyses of the spheres and examined the expression of EpCAM and α-fetoprotein (AFP), a hepatic stem/progenitor cell marker [16]. Although the DSF treatment decreased the number of cells positive for AFP or EpCAM, co-treatment with DSF and SB203580 restored the number of positive cells (Figure 4D and 4E). Taken together, DSF impaired the tumor-initiating capability of HCC cells in part in a p38-dependent manner.

Gene expression profiles of EpCAM$^+$ HCC cells treated with DSF

EpCAM$^+$ HCC cells treated with DSF or 5-FU for 48 hours were subjected to oligonucleotide microarray experiments. Concordant with the results presented in Figures 3 and 4, gene set enrichment analysis (GSEA) showed that EpCAM$^+$ HCC cells

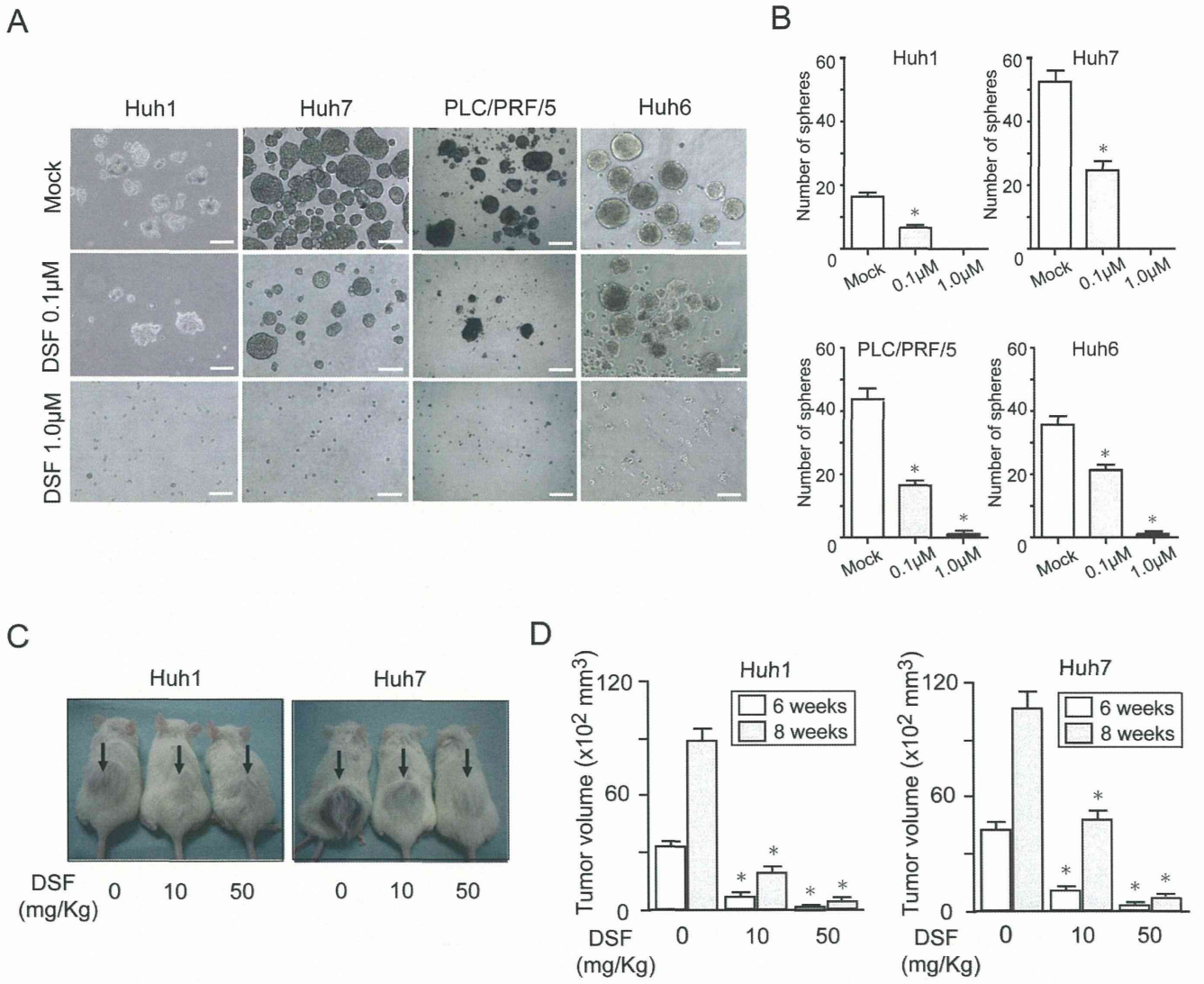

Figure 1. Sphere formation assays on HCC cells and xenograft transplantation. (A) Non-adherent sphere formation assay on HCC cell lines at day 14 of culture. Bright-field images are shown. Scale bar = 200 μm. (B) Number of large spheres generated from 1,000 HCC cells treated with DSF. *Statistically significant ($p<0.05$). (C) A total of 2×10^6 Huh1 or Huh7 cells were transplanted into the subcutaneous space of NOD/SCID mice. The growth of subcutaneous tumors (arrows) was apparently suppressed by the DSF treatment in a dose-dependent manner 8 weeks after transplantation. (D) Subcutaneous tumor volume was determined 6 and 8 weeks after transplantation. *Statistically significant ($p<0.05$).
doi:10.1371/journal.pone.0084807.g001

treated with DSF, but not 5-FU were significantly enriched for genes involved in p38-MAPK signaling (Figure 5A) [17,18]. The DSF treatment altered the expression of several genes involved in cell cycle regulation (Figure S6A and S6B). In particular, striking upregulation of *p57KIP2* was observed in Huh1 EpCAM$^+$ cells. The gene set for the proteasome pathway showed a higher enrichment score in DSF-treated EpCAM$^+$ HCC cells than in 5-FU-treated cells, although there was no significant difference (Figure S6C) [19].

We identified DSF-responsive genes (698 upregulated genes and 605 downregulated genes) and 5-FU-responsive genes (717 upregulated genes and 1,350 downregulated genes) (Figure 5B and 5C). Of interest, the DSF treatment causes no marked changes in the gene expression of the ROS scavenger pathway (Figure S6D). Furthermore, functional annotation analysis revealed different gene expression profiles between EpCAM$^+$ HCC cells treated with DSF and 5-FU (Table S1 and S2). In particular, gene ontology terms enriched for downregulated genes were different. Additionally, 23 genes categorized into "liver cancer" were downregulated after exposure to DSF, but not 5-FU (Figure 5D). Among them, Glypican3 (GPC3) was shown to be specifically overexpressed in human HCC and *GPC3*-knockdown induced apoptosis in HCC cells [20,21]. Quantitative RT-PCR showed that *GPC3* expression was downregulated in EpCAM$^+$ HCC cells treated with DSF as shown in the microarray analyses (Figure 5E). However, the downregulation of *GPC3* was not observed in EpCAM$^-$ HCC cells after DSF treatment (data not shown).

Regulation of *GPC3* gene expression

To examine whether activation of the ROS-p38 MAPK pathway was crucial to the downregulation of *GPC3* expression by DSF, we examined *GPC3* expression in EpCAM$^+$ HCC cells co-treated with NAC or SB203580. Neither NAC nor SB203580

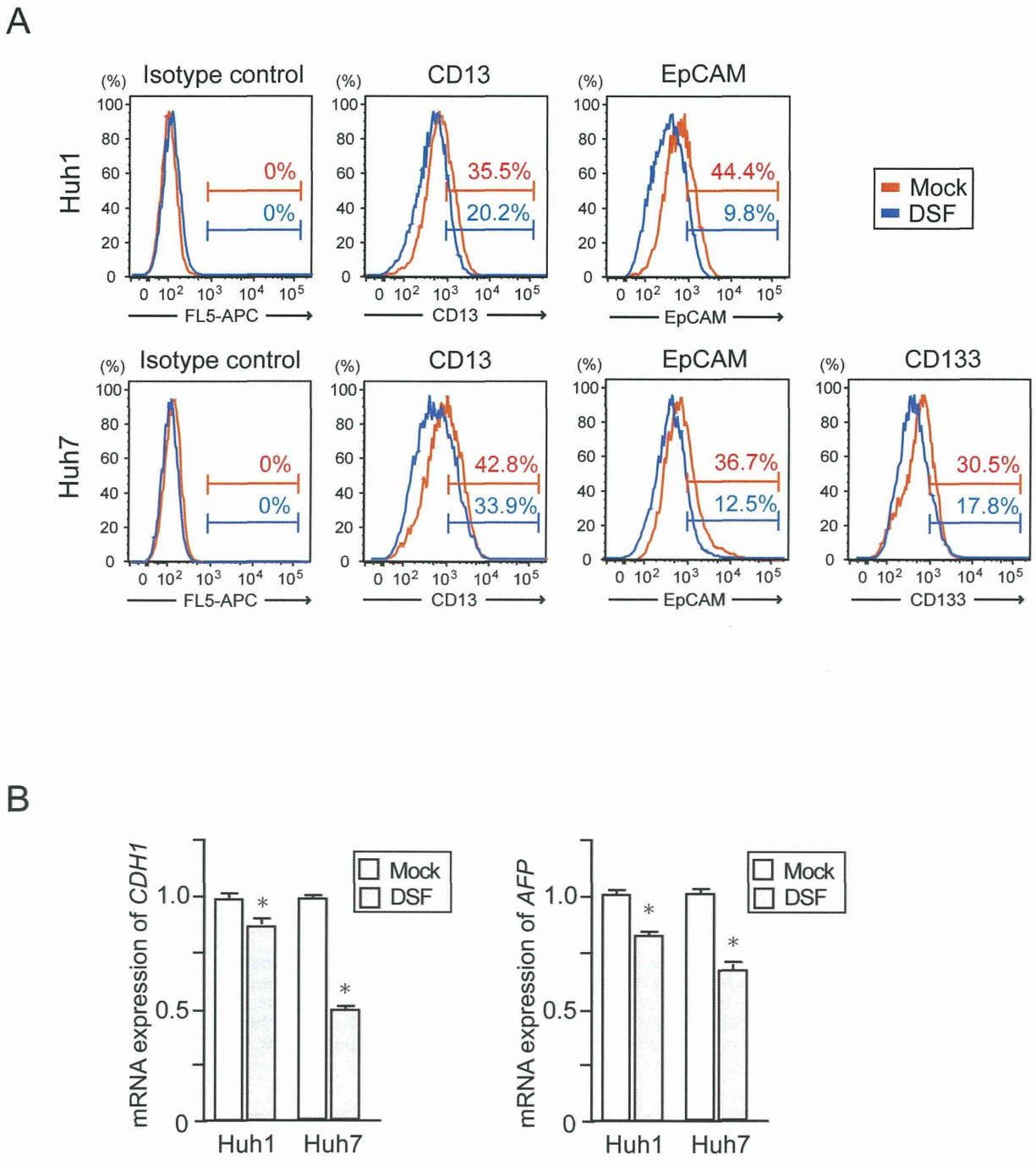

Figure 2. Flow cytometric analyses and quantitative RT-PCR analyses of HCC cells treated with DSF. (A) Flow cytometric profiles in Huh1 and Huh7 cells treated with DSF (0.1 μM) for 48 hours. The percentages of positive fractions for indicated markers are shown as the mean values for three independent analyses. (B) Real-time RT-PCR analyses of hepatic stem/progenitor cell marker genes. *Statistically significant ($p<0.05$).
doi:10.1371/journal.pone.0084807.g002

restored the expression of *GPC3* (Figure S7A). In addition, proteasome inhibition by the MG132 treatment had no effect on *GPC3* expression (Figure S7B). These findings indicate that neither ROS-p38 MAPK pathway activation nor proteasome inhibition contributed to the downregulation of *GPC3* expression.

Loss-of-function and gain-of-function assays of GPC3 in EpCAM$^+$ HCC cells

Dual immunostaining analyses showed that GPC3 and EpCAM were frequently co-expressed in HCC cells (Figure 6A). Moreover, quantitative RT-PCR revealed a higher level of GPC3 expression in the EpCAM$^+$ fraction than in the EpCAM$^-$ fraction (Figure 6B). Stable HCC cell lines expressing shRNA against *GPC3* or *luciferase* were successfully obtained by cell sorting with enhanced green fluorescent protein (EGFP) as a marker for viral infection. Western

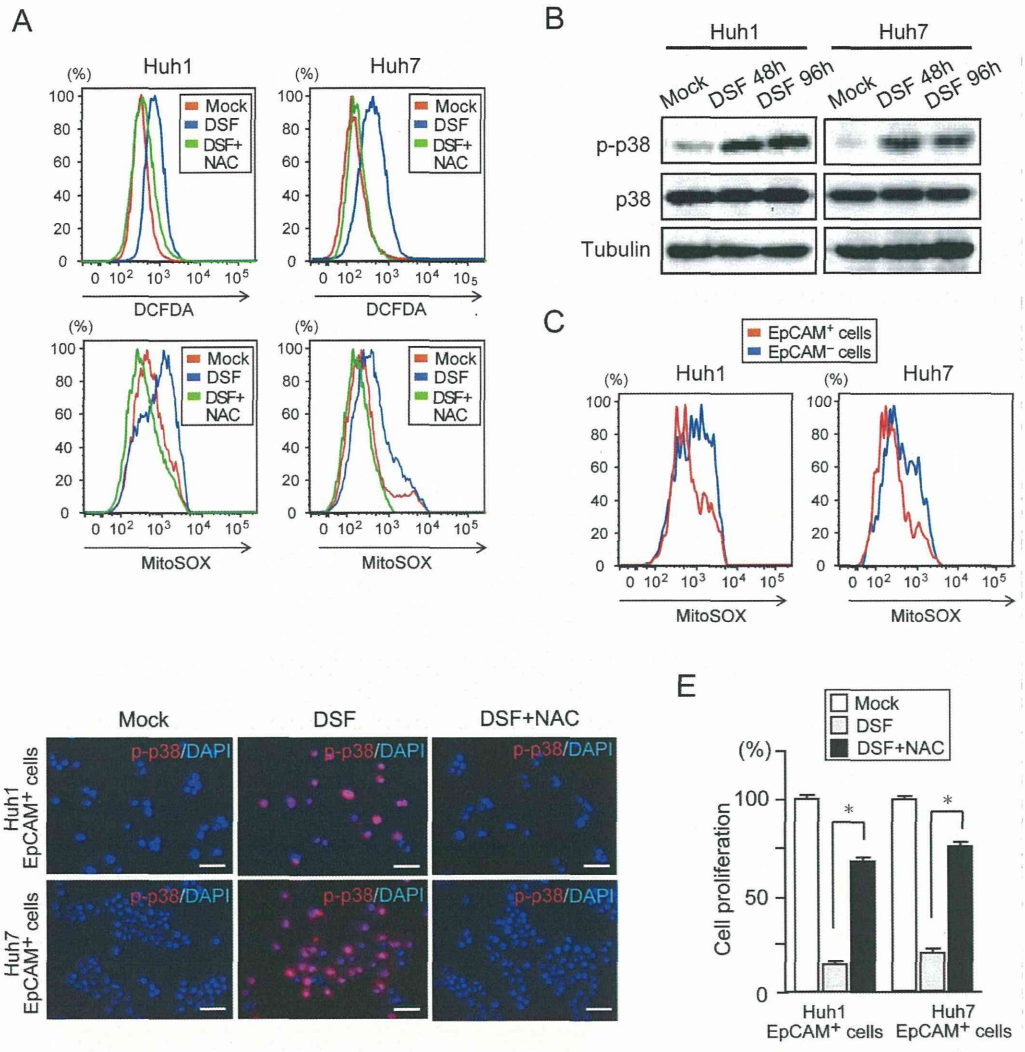

Figure 3. Activation of the ROS-p38 MAPK pathway in tumor-initiating EpCAM$^+$ cells treated with DSF. (A) Flow cytometric analysis of ROS levels. Intracellular ROS concentrations were measured by DCFDA and MitoSOX staining. (B) Cells treated with DSF for 48 or 96 hours were subjected to Western blot analysis using phospho-p38 (p-p38), p38, and anti-tubulin (loading control) antibodies. (C) Flow cytometric analysis of ROS levels in view of EpCAM expression. Intracellular ROS concentrations were measured by MitoSOX staining. (D) Fluorescence images of EpCAM$^+$ HCC cells. The expression of p-p38 (red) was merged with nuclear DAPI staining (blue). Scale bar = 100 μm. (E) Proliferation of EpCAM$^+$ HCC cells at 96 hours in culture. The percentages of cells are shown. *Statistically significant ($p<0.05$).
doi:10.1371/journal.pone.0084807.g003

blot analysis of these cells showed that both shRNAs against *GPC3* (sh-*GPC3*-1 and sh-*GPC3*-2) markedly repressed GPC3 expression, although sh-*GPC3*-1 was more effective than sh-*GPC3*-2 (Figure 6C). *GPC3*-knockdown suppressed cell growth and induced apoptosis relative to sh-*Luc* (Figure S7C and S7D). Similarly, *GPC3*-knockdown markedly impaired primary sphere formation by EpCAM$^+$ cells and EpCAM$^-$ cells and more severely impaired secondary sphere formation (Figure 6D-F). Immunocytochemical analyses of the large spheres showed a decrease in the number of cells expressing AFP or EpCAM (Figure S7E and S7F). In contrast, the stable overexpression of *GPC3* promoted cell growth and sphere formation of tumor-initiating HCC cells (Figure S8). Together, these results indicate that *GPC3*-knockdown suppresses tumorigenicity of HCC cells by directly affecting the cell growth and the self-renewal of TIC.

Discussion

High levels of ALDH activity are characteristic of normal stem cells in a variety of organs. The human ALDH superfamily consists of 19 putatively functional genes [22]. ALDH1 is a major isoform in mammalian tissues and functions as a stem cell marker in liver and mammary stem cells [23,24]. Recent reports have indicated ALDH1 to be a useful marker for the enrichment of TICs from various cell lines and primary tumors. It has been shown that a high level of ALDH1 expression correlates with malignant phenotypes and an unfavorable prognosis in a range of cancers [24].

In this study, we first showed that DSF inhibited the proliferation and sphere-forming ability of HCC cells in a dose-dependent manner. In addition, DSF suppressed tumor growth in xenograft transplant experiments using NOD/SCID mice. Our flow cytometric analysis showed that the DSF treatment caused a significant decrease in the number of tumor-initiating HCC cells

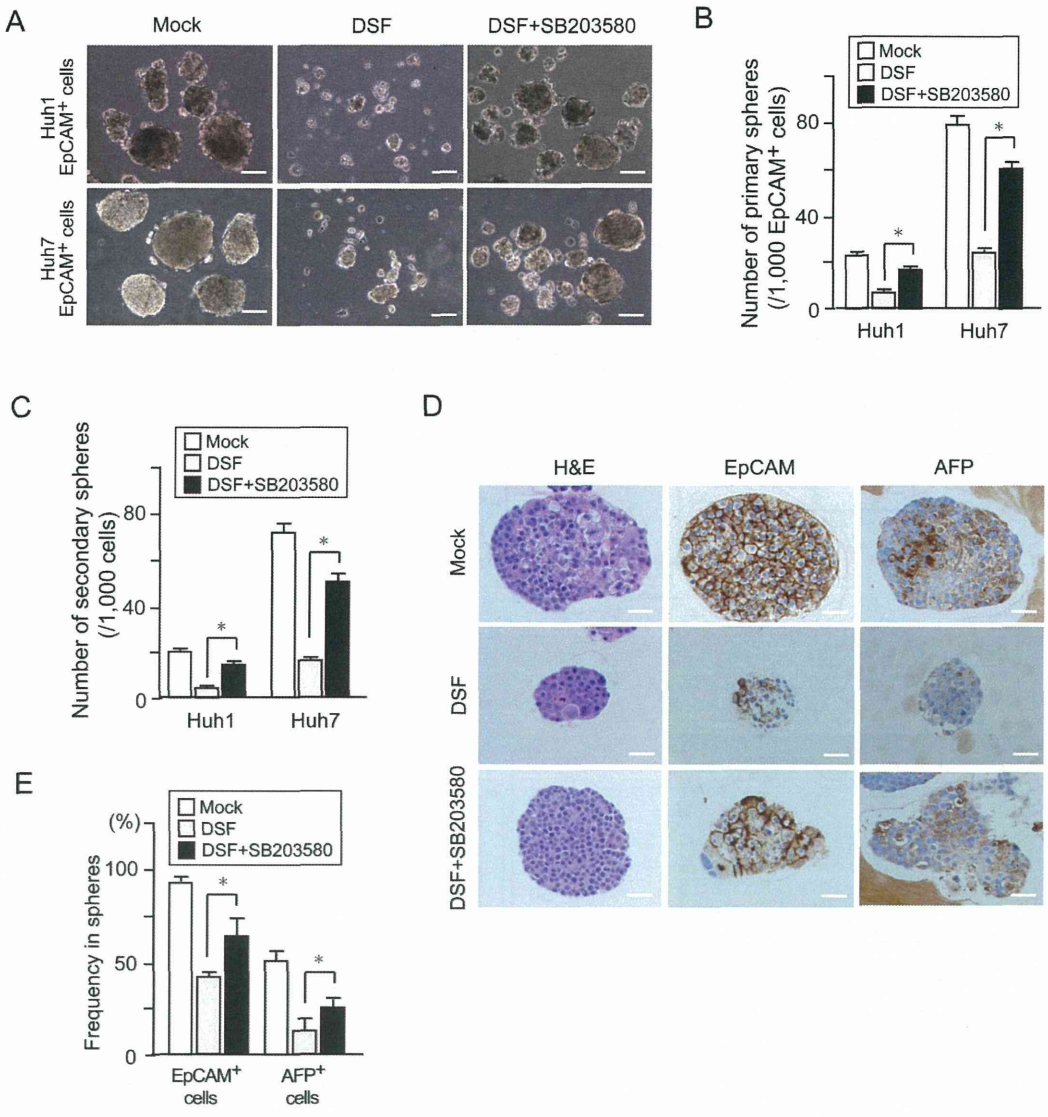

Figure 4. Sphere formation assays and immunocytochemical analyses in tumor-initiating EpCAM$^+$ cells treated with a p38 inhibitor (SB203580). (A) Bright–field images of non-adherent spheres on day 14 of culture. Scale bar = 100 μm. (B) Number of large spheres derived from 1,000 EpCAM$^+$ tumor cells on day 14 of culture. *Statistically significant ($p<0.05$). (C) Number of secondary spheres 14 days after replating. *Statistically significant ($p<0.05$). (D) H&E staining and immunocytochemical analysis of EpCAM and AFP in spheres derived from EpCAM$^+$ cells. (E) Quantification of the percentage of EpCAM$^+$ cells or AFP$^+$ cells. *Statistically significant ($p<0.05$).
doi:10.1371/journal.pone.0084807.g004

expressing surface markers such as CD13, CD133, and EpCAM. Knockdown of *ALDH1* and *ALDH2* in HCC cells had no effect on cell proliferation and sphere-forming ability in the culture. Our findings suggest that DSF exerts its anti-HCC function in an ALDH-independent fashion.

HSCs have been shown to tightly control intracellular ROS levels to maintain long-term self-renewal and survival [25]. Conversely, activation of p38 MAPK upon an elevation in ROS levels resulted in the exhaustion of HSCs [26]. Similarly, TICs in a wide range of tumors exhibited lower concentrations of ROS than corresponding non-TICs. In addition, lower ROS levels in TICs were shown to be closely associated with both chemo-sensitivity and radio-sensitivity [15]. In the present study, we confirmed that EpCAM$^+$ HCC cells contained lower ROS levels than EpCAM$^-$ cells. Because previous studies reported that DSF activated the ROS-p38 MAPK pathway and thereby suppressed the sphere-forming ability of TICs [6,7], we examined whether exposure to DSF activated the ROS-p38 MAPK pathway in tumor-initiating HCC cells. As expected, the treatment of EpCAM$^+$ HCC cells with NAC canceled p38 activation. Moreover, the SB203580 treatment largely restored the tumorigenicity of EpCAM$^+$ HCC cells. These findings indicate that the ROS-p38 MAPK pathway is directly associated with cell growth and tumor-initiating capability of HCC cells. Low levels of ROS in TICs have been attributable to the activation of the ROS scavenger pathway [27]. The present microarray results showed comparatively high expression levels of ROS scavenger genes such as *GCLM* and *GSS* in purified EpCAM$^+$ HCC cells. However, the DSF treatment caused no marked changes to the ROS scavenger genes. Considering that not only H2DCFDA staining but also MitoSOX staining showed a high ROS level in DSF-treated EpCAM$^+$ HCC cells, DSF might increases mitochondrial ROS production rather than impairs the scavenging of ROS. Further analysis is required to clarify this point.

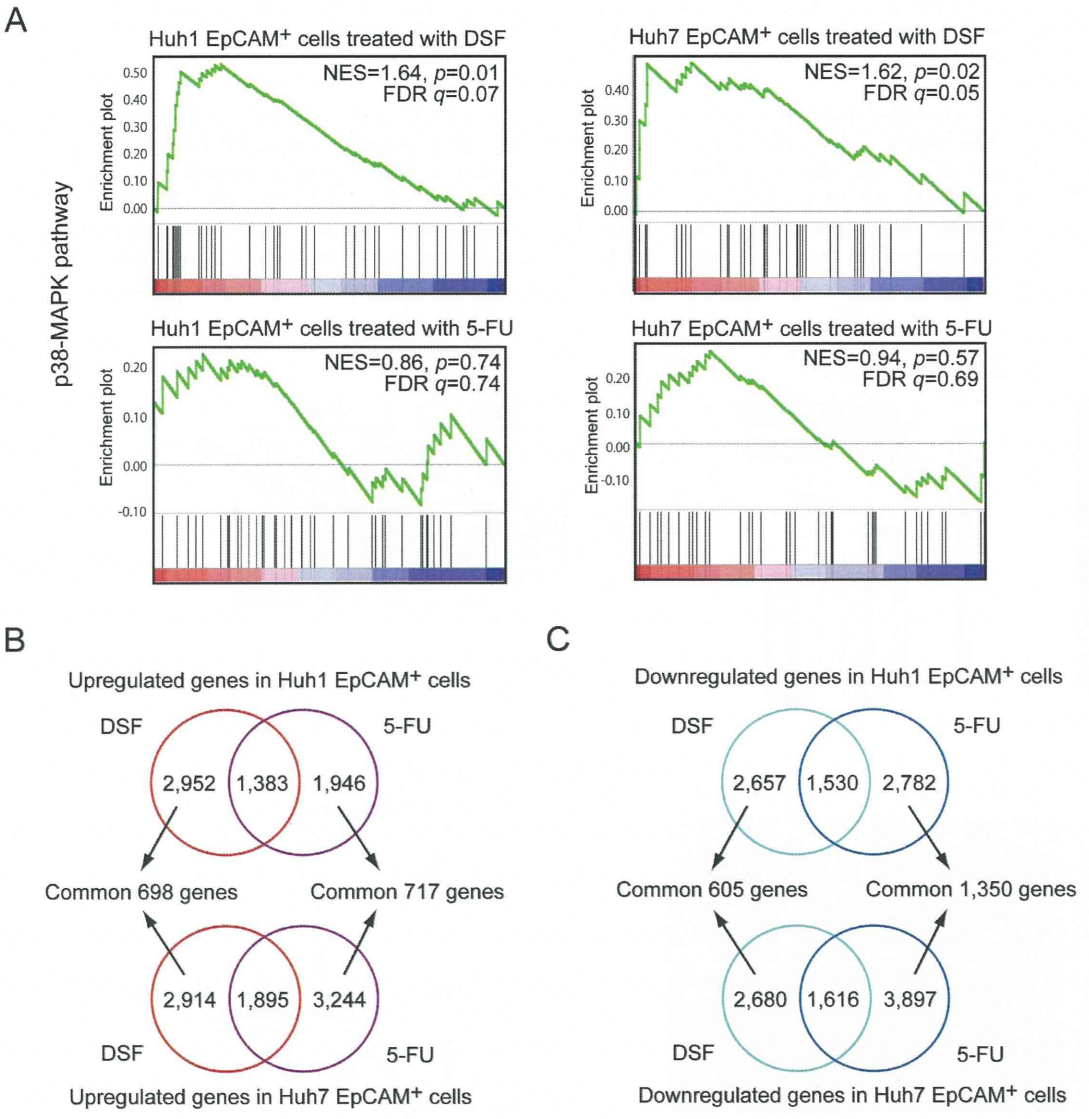

D

Downregulated genes annotated as "liver cancer" in functional analysis

UniGene	Symbol	UniGene	Symbol
Hs.442182	ABCC6	Hs.426485	HPX
Hs.334707	ACY1	Hs.524513	HSD17B6
Hs.530274	ALDOB	Hs.282735	NR1H4
Hs.052968	APOA5	Hs.654800	PNPLA3
Hs.461086	CDH1	Hs.525557	SERPINA1
Hs.84113	CDKN3	Hs.436893	SLC15A1
Hs.647036	CLDN4	Hs.656544	SOAT2
Hs.129798	DGAT2	Hs.71465	SQLE
Hs.304682	CST3	Hs.478265	TNFSF10
Hs.118681	ERBB3	Hs.351815	TPD52
Hs.333303	GJB1	Hs.108049	UACA
Hs.644108	GPC3		

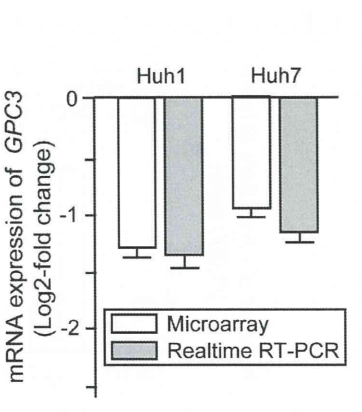

Figure 5. Gene expression profiles of EpCAM$^+$ cells treated with DSF or 5-FU. (A) Gene set enrichment analysis (GSEA) of the p38-MAPK signaling pathway. Both the normalized enrichment score (NES) and false discovery rate (FDR) are shown in each enrichment plot. (B) Common upregulated genes in Huh1 cells (upper panel) and Huh7 cells (lower panel) after DSF or 5-FU treatment are depicted in Venn diagrams. (C) Common downregulated genes in Huh1 cells (upper panel) and Huh7 cells (lower panel) after DSF or 5-FU exposure are depicted in Venn diagrams. (D) A list of

downregulated genes annotated as "liver cancer" in DSF-treated EpCAM$^+$ HCC cells. (E) The expression of *GPC3* in DSF-treated EpCAM$^+$ cells was compared to that in control cells. The data obtained by microarray analyses and quantitative RT-PCR analyses are presented.
doi:10.1371/journal.pone.0084807.g005

Of interest, our microarray analyses revealed that DSF acted in a manner different from 5-FU. The GSEA results support the present biological finfings and implicate the activation of p38 in the anti-TIC activity of DSF. Importantly, the 23 genes in the "liver cancer" category were significantly downregulated after the DSF exposure, but none of them was significantly altered after the 5-FU treatment. One of these genes, GPC3, was frequently overexpressed in HCC and increased GPC3 expression was correlated with a poor prognosis among HCC patients [20,21]. A clinical trial using a GPC3 peptide vaccine in patients with advanced HCC has also been carried out [28]. While GPC3 functions as a marker for normal hepatic stem/progenitor cells [29], the immunostaining analyses showed an association between the expression of EpCAM and GPC3 in both HCC cell lines and

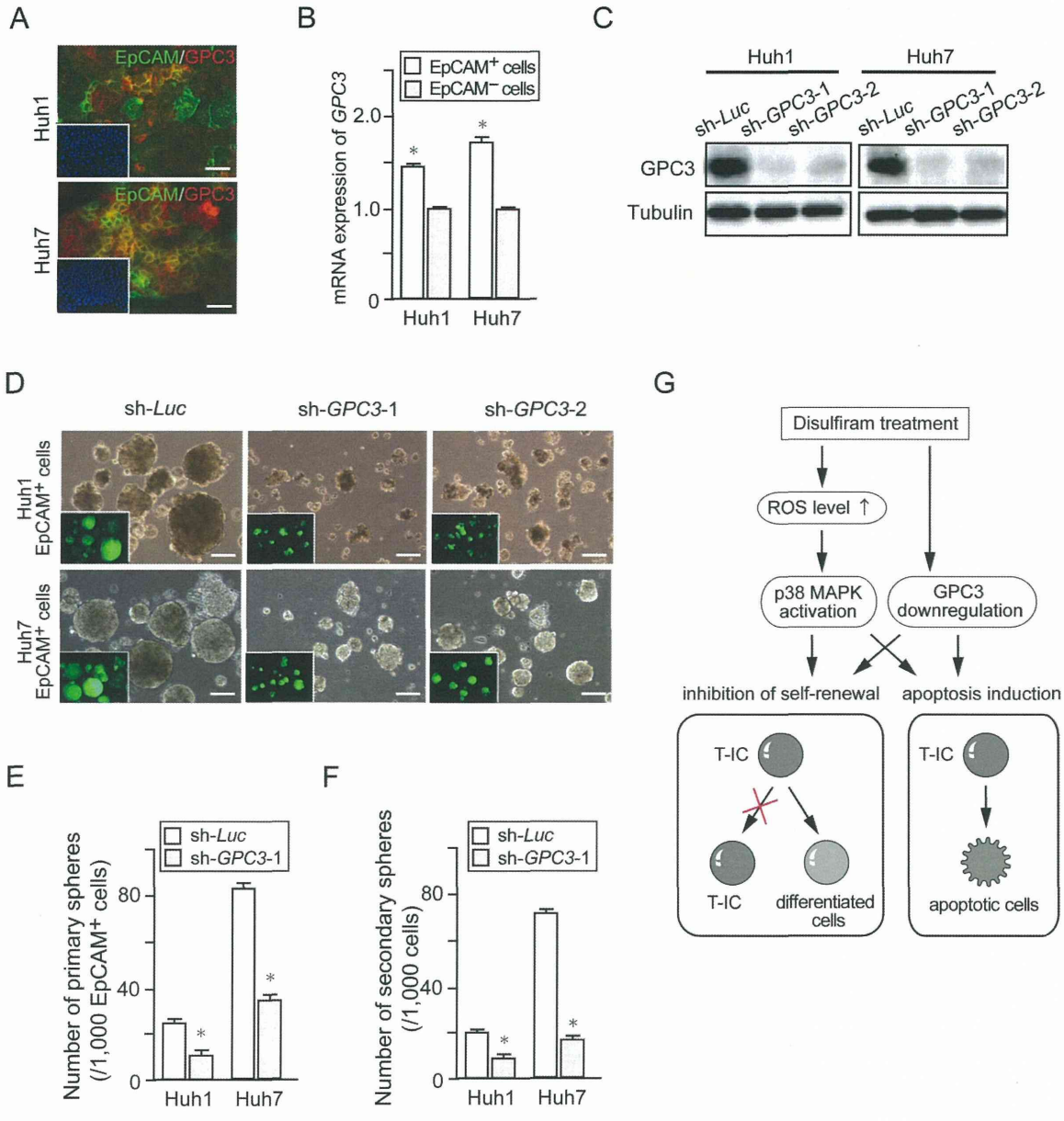

Figure 6. Impact of *GPC3* depletion on sorted EpCAM$^+$ HCC cells. (A) Dual immunostaining was performed to detect the expression of EpCAM (green) and GPC3 (red). Nuclear DAPI staining is shown in the insets. Scale bar = 100 μm. (B) Real-time RT-PCR analysis of GPC3 expression in purified EpCAM$^+$ cells. *Statistically significant ($p<0.05$). (C) Cells transduced with the indicated lentiviruses were subjected to Western blotting using anti-GPC3 and anti-tubulin (loading control) antibodies. (D) Bright–field images of non-adherent spheres on day 14 of culture. Fluorescence images are shown in the insets. Scale bar = 100 μm. (E) Number of large spheres derived from 1,000 EpCAM$^+$ or EpCAM$^-$ cells at day 14 of culture. *Statistically significant ($p<0.05$). (F) Number of secondary spheres 14 days after replating. *Statistically significant ($p<0.05$). (G) A proposed model for the effect of DSF in targeting tumor-initiating HCC cells.
doi:10.1371/journal.pone.0084807.g006